# Dependence of the optical and magneto-optical properties and electronic structures on the atomic order in $Ni_2MnIn$ Heusler alloys

Y. V. Kudryavtsev
*Institute of Metal Physics, National Academy of Sciences of Ukraine, Kiev-142, Ukraine*

Y. P. Lee*
*Quantum Photonic Science Research Center and Department of Physics, Hanyang University, Seoul 133-791, Korea*

J. Y. Rhee
*Department of Physics, Hoseo University, Asan, Choongnam 336-795, Korea*

(Received 4 December 2003; revised manuscript received 24 February 2004; published 13 May 2004)

The magnetic, the magneto-optical, and the optical properties of $Ni_2MnIn$ alloy films with significantly different atomic orders (from nearly single crystalline to highly disordered or almost amorphous) were investigated. The crystalline $Ni_2MnIn$ alloy films were ferromagnetic with a Curie temperature of 325–330 K, while the amorphous phase was not ferromagnetically ordered down to 5 K. The diagonal and off-diagonal components of the optical-conductivity tensor for the crystalline alloy were experimentally determined. They were also calculated by using an all-electron full-potential linearized-augmented-plane-wave method and the agreement between the experiment and calculation was reasonable after the so-called λ fitting. The most intense optical transitions occur between the minority-spin bands with mostly Ni and/or Mn 3*d* characters. The joint-density-of-states effects are responsible for these transitions. The analysis of changes in the electron-energy structure of $Ni_2MnIn$ alloy, caused by the structural disordering, were performed by using the results of optical study. An annealing at 750 K for 2 h of the amorphous film restores its crystallinity ($B2$ or $A2$ phases) and also the ferromagnetic order.

DOI: 10.1103/PhysRevB.69.195104 PACS number(s): 78.20.Ci, 78.20.Ls, 71.20.Be

## I. INTRODUCTION

The rapidly evolving field of magnetoelectronics stimulates deep interests in ferromagnetic metals with full spin polarization at the Fermi level $E_F$. This phenomenon may be observed in compounds which are thought to be metallic for one-spin direction, while at the same time they show semiconducting properties for the opposite spin direction. These so-called half-metallic ferromagnets are favorable candidates as electrodes for spin-polarized-current injection into semiconductors. A significant number of intermetallic semi-Heusler and true Heusler alloys (HA) have been predicted theoretically to be half metals[1] and their films may be used as spin injectors in such devices. True HA have a formula of $X_2YZ$, where $X$ and $Y$ are transition metals and $Z$ is an $s$-$p$ element and they are in a crystalline structure of $L2_1$. Recent experiments, however, indicate that when using HA as electrodes on semiconductor material, the spin polarization of the injected carriers is far from complete.[2] This is thought to be related to poor interface properties (both electrical and magnetic) due to site disorder, resulting in an insufficient spin polarization of the ferromagnet at $E_F$. Indeed, the full spin polarization at $E_F$ was theoretically predicted only when assuming a perfectly ordered $X_2YZ$ structure with a pure $L2_1$ type of symmetry.[3] It was also theoretically shown for several HA [such as $Rh_2MnZ$ ($Z$=Ge, Sn, Pb) or $Cu_2NiZn$] that a pseudogap in the density of states (DOS) for minority-spin subbands disappeared in the disordered state.[4,5]

For example, the magnetic measurements of $Co_2MnZ$ ($Z$=Sn, Si, Ge) alloy films[6,7] reveal that, depending on the specific combination of substrate materials and the film thickness, the saturation magnetization is strongly reduced compared to the bulk value. Evidently, for a thickness below approximately 15 Åsuch HA films are no longer ferromagnetic. This result indicates that typically several monolayers of the HA at an interface are not ferromagnetic, probably owing to alloying or strong site disorder.

However, the origin of ferromagnetism, and the effect of atomic disorder on the electronic structure and the physical properties of HA is still not well understood and constitutes a challenging problem. It is well known that the cold working, as well as an atomic disordering or a compositional deviation from the stoichiometry, changes the magnetic properties of HA (see, for example, Refs. 8 and 9). The magnetic moment in Mn-containing HA is predominantly located at the Mn sites. Because the Mn atoms in the ordered HA are widely separated by the nonmagnetic $Z$ atoms, the Mn atoms have been considered to be coupled via the conduction electrons by a Ruderman-Kittel-Kasuya-Yosida $s$-$d$ interaction. Therefore, any change in the chemical or the atomic order may directly influence the magnetic behavior of the alloy. Ikeda and Takahashi[8] considered the effect of formation of antiphase boundaries produced by a plastic deformation and showed that the saturation magnetization as well as the Curie temperature $T_C$ could be reduced by about 30% if the dislocation density reached a value of about $10^{13}$ cm$^{-2}$. Pugacheva and Jezierski[4] have shown theoretically that the structural disordering in $Rh_2MnZ$ ($Z$=Ge, Sn, Pb) HA reduces the magnetic moment by about 11%. At the same time, Taylor and Tsuei[10] as well as Krusin-Elbaum *et al.*[11] have shown that a significant structural disordering obtained in

 

TABLE I. The parameters of the investigated $Ni_2MnIn$ alloy bulk and film samples. $T_s$ and $t$ are substrate temperatures during the deposition and film thickness, respectively. $4\pi M_{eff}$ were measured at 293 K.

| Sample no. | $T_s$ (K) | Heat treatment | $t$ (nm) | Mean-grain size (nm) | Lattice constant (Å) | FWHM of (220) peak (deg) | $4\pi M_{eff}$ (G) | $T_C$ (K) |
|---|---|---|---|---|---|---|---|---|
| Bulk | | | | | 6.076 | 0.30 | | 317 |
| 1 | 730 | | 135 | 80–90 | $a=6.185,\ c=6.076$ | 0.76 | 1790 | 330 |
| 2 | 680 | | 130 | | $a=6.189,\ c=6.060$ | 0.80 | 773 | |
| 3 | 545 | | 105 | 20–30 | $a=6.159,\ c=6.118$ | 0.86 | 247 | |
| 4 | 150 | | 75 | $<2\sim3$ | | 3.40 | 0 | |
| 5 | 150 | 750 K/2 hr | 243 | | $a=6.188,\ c=6.095$ | 0.73 | 743 | 325 |

amorphous $Cu_2MnZ$ ($Z$=Al, In, Sn) HA films will lead to the formation of a spin-glass state. On the other hand, amorphous $Ni_2MnGa$ alloy films exhibit a feature of Pauli paramagnet down to the liquid-He temperature.[12] Unlike the preceding cases, Ślebarski *et al.*[13] have shown that the atomic disordering in $Fe_2TiSn$ HA causes the appearance of a weak ferromagnetism in the nonmagnetic ordered state.

The spin-injector layer has to satisfy several demands: an excellent lattice matching to the semiconductor layer as well as a good matching between their band structures. The ordered stoichiometric bulk $Ni_2MnIn$ alloy has a cubic $L2_1$ crystal structure with a lattice constant $a$ of 6.069 Å (or 6.073 Å) (Ref. 14) and a $T_C$ of 314 K (Refs. 15,16) [or 320 K (Ref. 14)]. The lattice constant is very close to that of semiconducting InAs (i.e., $a=6.058$ Å). This fact makes them a promising couple for the spintronic devices. Kilian and Victora[17] have shown that $Ni_2MnIn$ also has a good band matching with InAs in three high-symmetry directions, among which the [111] direction is the best.

The magneto-optical (MO) spectroscopies are rather sensitive and convenient tools in studying the electronic structure and the magnetic properties of magnetically ordered solids at the same time. The MO and optical properties as well as the electronic structures of semi-Heusler[18–27] and true Heusler alloys[28–33] were intensively studied experimentally and theoretically. However, the dielectric function (DF) of $Ni_2MnIn$ alloy (as far as we know) has not been investigated yet either experimentally or theoretically. It is very attractive to apply the thin-film technology to obtain the $Ni_2MnIn$ alloy in structurally different states (from rather ordered to essentially disordered one) in order to elucidate the overall structural dependence of the electronic structure and the magnetic properties. Thus, this work aims at the fabrication of $Ni_2MnIn$ alloy films in structurally different states, and the investigation on the influence of atomic ordering in $Ni_2MnIn$ alloy on the magnetic, the MO and the optical properties as well as the electronic structure. The MO and optical properties were also calculated by using first-principles electronic-structure calculations and the agreement with experiment was reasonable.

## II. EXPERIMENTAL PROCEDURE

Bulk $Ni_2MnIn$ alloy was prepared by melting Ni, Mn, and In pieces of 99.99 purity together in an arc furnace with a water-cooled Cu hearth in an Ar atmosphere at the pressure of 1.3 atm. Before preparation of the $Ni_2MnIn$ ingot, the Ar gas in the furnace was additionally purified by multiple remelting of $Ti_{0.50}Zr_{0.50}$ alloy getter. To promote volume homogeneity the ingot was remelted times times. Any weight loss after melting was not observed. The x-ray fluorescence analysis revealed an alloy composition of $Ni_{0.502}Mn_{0.248}In_{0.250}$ with error margins of about 0.3 wt% (hereafter we refer to this as $Ni_2MnIn$). For the optical and MO measurements a slab of about $15\times8\times2$ mm$^3$ in dimensions was cut from the ingot using spark-erosion technique and then polished mechanically with diamond powders. The final stage of the mechanical polishing was carried out with the use of the water suspension of $Cr_2O_3$. Then, the sample surface was cleaned with acetone and ethanol using an ultrasonic cleaner and put into a vacuum chamber for the optical measurements. To remove the surface contamination introduced by the mechanical treatment, the sample was annealed in a high-vacuum condition at 720 K for 3 h.

$Ni_2MnIn$ alloy films of $10\times30$ mm$^2$ in dimensions with different degrees of structural order were prepared by flash evaporation of the crushed alloy powders of 80–100 $\mu$m in diameter simultaneously onto glass and NaCl substrates in a vacuum better than $2\times10^{-5}$ Pa. The alloy powder was prepared from the same ingot of bulk $Ni_2MnIn$ alloy. To obtain highly ordered films, the deposition was performed onto substrates heated up to 730 K, while the utmost disordered (for our case) alloy films were prepared by vapor-quenching deposition onto substrates cooled by liquid nitrogen. The actual substrate temperature during quenching deposition was estimated to be 150 K. Additionally, some latter films were annealed *in situ* at 750 K for 2 h. The deposition onto substrates kept at the temperatures in between 150 and 730 K allowed us to fabricate the alloy films with intermediate degrees of structural order. The parameters of the prepared $Ni_2MnIn$ alloy films are summarized in Table I.

The structural characterization of the bulk and film $Ni_2MnIn$ alloy samples was carried out by using $\Theta-2\Theta$ and grazing-angle x-ray diffraction (XRD) study with Cu and Fe $K_\alpha$ radiation, and by using the selective-area microdiffraction of transmission electron microscopy (TEM) for the films on NaCl substrates. The optical properties of $Ni_2MnIn$ samples were measured by using a rotating-analyzer spectroscopic ellipsometer at room temperature (RT) in a spectral range 265–2500 nm (4.7–0.5 eV) at a fixed incidence angle

of 73°. The MO properties (equatorial Kerr effect: EKE, $\delta_p$) of the $Ni_2MnIn$ HA were investigated at RT by the dynamical method using *p*-plane polarized light at two angles of incidence (66° and 75°) in a spectral range 290–1100 nm (4.20–1.05 eV). The temperature dependence of the magnetic properties was investigated by measuring the dc magnetic susceptibility $\chi(T)$ under an external field of 100 G in the 77–395 K temperature range. The magnetic properties of $Ni_2MnIn$ alloy films [in plane, zero-field-cooled (ZFC) and field-cooled (FC), $H=100$ G, magnetization curves as well as magnetization hysteresis loops] were studied by using a Quantum Design superconducting quantum interference device (SQUID) magnetometer in the 5–395 K temperature range. Additionally, the magnetic state of the film samples at RT was evaluated by measuring the ferromagnetic resonance (FMR) for the in-plane and out-of-plane geometries.

## III. THEORETICAL CALCULATIONS

The electronic structures were calculated by using the WIEN2K code[34] utilizing an all-electron full-potential linearized-augmented-plane-wave method.[35] For the exchange-correlation functional, the generalized-gradient-approximation version of Perdew, Burke, and Ernzerhof[36] was used. Since the spin-orbit coupling is crucial for the MO effects, it is included in a second-variational procedure, and the eigenvalues and eigenvectors are computed using scalar-relativistic wave functions. The muffin-tin radii were determined in such a way that all atomic spheres were almost in contact and were the same for all atoms. We used $RK_{\max}=8.0$, resulting in 330 plane waves for the basis functions. To generate the self-consistent potential and charge, we divided the whole reciprocal unit cell into $10\times10\times10$ parallelepipeds, resulting in 102 independent **k** points in an irreducible wedge. It should be noted here that the inclusion of the spin-orbit interaction reduced the symmetry of the crystal from cubic to tetragonal in the spin-polarized calculations. After self-consistency was achieved, the whole reciprocal unit cell was further divided into $40\times40\times40$ parallelepipeds, resulting in 4531 independent **k** points in an irreducible wedge, and the energy eigenvalues and eigenfunctions were obtained to calculate the DOS curves and the optical-conductivity (OC) spectra. A detailed explanation for the OC calculation can be found elsewhere.[37]

The calculated OC spectra were broadened using a Lorentzian function with a lifetime of 0.3 eV. The broadening simulates the effects of the imaginary part of the quasiparticle self-energy and the instrumental resolution. Since the calculated spectra after broadening have similar shapes to the measured ones but the energy positions of the strong features are different, we applied the real part of the self-energy correction (so-called λ fitting[38]) to match the energy positions of the strong features of the experimental and theoretical spectra. The detailed explanation of the λ fitting and fitting procedures can be found elsewhere.[38,39] All the calculations were done for the perfectly ordered $L2_1$ structure.

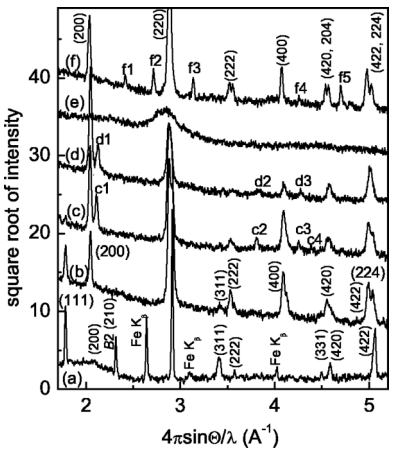


FIG. 1. XRD patterns for (a) bulk and thin-film $Ni_2MnIn$ alloy samples deposited at (b) 730, (c) 660, (d) 545, (e) 150 K. XRD spectrum for the film deposited at 150 K and annealed at 750 K for 2 h is shown as curve (f).

## IV. RESULTS AND DISCUSSION

### A. Structural and magnetic properties

Different kinds of atomic orders in true HA may be observed. The completely ordered state is the $L2_1$ structure, in which a linear chain of Ni-Mn-Ni-In lies along the (111) direction of *bcc*-based structure, forming a *fcc* Bravais lattice. The $B2$ structure occurs when Ni atoms occupy their proper sites, while Mn and In atoms randomly occupy their sites (centers of cubic cages of Ni atoms). And finally random occupation of the sites of *bcc* lattice by Ni, Mn, and In atoms produces the $A2$ structure. The structural homogeneity of the investigated bulk sample was proven to be practically a single phase: all the observed diffraction lines belong to the $L2_1$ phase, except the (210) one whose presence can be a consequence of a certain disorder of the $B2$ structure (see Fig. 1). From the *d* spacings, the lattice parameter of bulk $Ni_2MnIn$ alloy turns out to be $6.076\pm0.021$ Å which is in close agreement with the literature value.[15]

The $Ni_2MnIn$ alloy films deposited onto substrate at 730 K show a well ordered single phase $L2_1$ structure with a small tetragonal distortion, $a=6.185$ Å and $c=6.076$ Å, and a rather large mean-grain size of 80–90 nm (see Figs. 1 and 2, and Table I). It should be noted that the (111) superstructural diffraction line of $L2_1$ phase was observed only in the XRD spectra of bulk sample and the film deposited at 730 K.

A decrease in the substrate temperature from 730 to 660 K and then down to 545 K still preserves the crystalline structure (see Figs. 1 and 2). However, main diffraction lines become wider (see Table I), and a few additional (in comparison with the $L2_1$ phase) diffraction lines marked by $c_i$ and $d_i$ have appeared (see Fig. 1). The new $c_1$ and $d_1$ peaks can be attributed to the (101) peak of $Ni_2In$ or the (310) peak of $Mn_3In$, while other peaks may be related to the formation of $B2$ structure [$c_2$ and $d_2$ to the (321), $c_3$ and $d_3$ to the (410) or (223), and $c_4$ to the (141) or (303) diffraction peaks]. The peaks $c_2$ and $d_2$ may also be originated from the (112) peak of $Ni_2In$. This is also accompanied by a noticeable reduction in mean-grain size of the films (see Table I

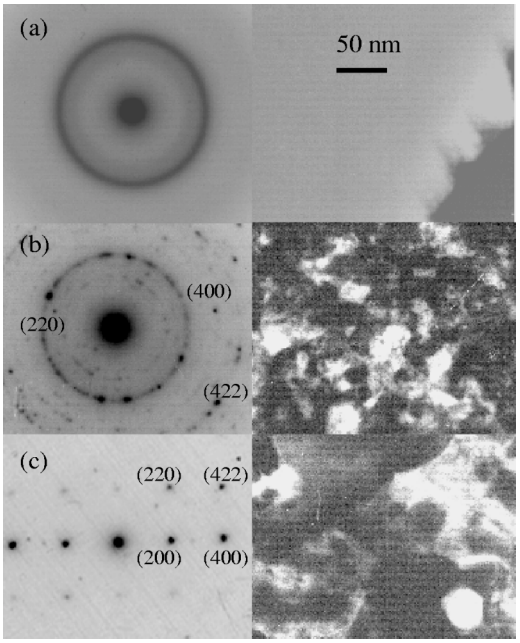


FIG. 2. TEM results for the $Ni_2MnIn$ alloy films deposited onto NaCl substrates at (a) 150 K, (b) 545 K, and (c) 730 K.

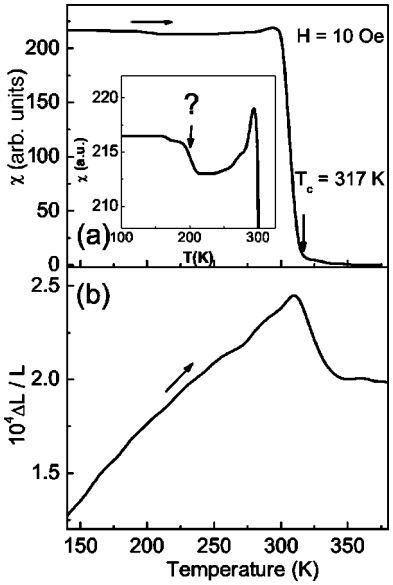


FIG. 3. Temperature dependence of (a) magnetic susceptibility $\chi(T)$ and (b) of the coefficient of expansion for bulk $Ni_2MnIn$ alloy. Inset in panel (a) shows an extended view of $\chi(T)$.

and Fig. 2). Finally, the quenching deposition onto substrates cooled by liquid nitrogen leads to the formation of highly disordered alloy films with only a smeared halo in the TEM diffraction patterns and the mean-grain size, if any, less than resolution threshold of the used TEM technique (see Fig. 2). The XRD spectrum of the highly disordered alloy films exhibits only a wide and weak peak around the (220)-peak position [see the spectrum (e) of Fig. 1]. An annealing of such films with a rate of 3 K/min causes a rapid decrease in their resistance near 620 K (not shown). Such a behavior is more typical for the crystallization of an amorphous film than for the recrystallization of a fine-grained polycrystalline film. Thus, one can conclude that vapor-quenching deposition onto substrates cooled by liquid nitrogen leads to the formation of an amorphous structure in the $Ni_2MnIn$ alloy films. *In situ* annealing of the amorphous films at 750 K for 2 h recovers the crystalline structure with a $B2$ type of order [see Fig. 1(f)]. However, in addition to the lines of $B2$ phase [i.e., to $f_4$—(410 or 223) and $f_5$—(124 or 142)] new diffraction lines of $f_1$–$f_3$ are clearly seen. They may be attributed to Mn oxides: $f_1$—(111) MnO, $f_2$—(222) $MnO_2$, and $f_3$—(003) $MnO_2$.

Magnetic measurements revealed a $T_C$ of 317 K for the bulk alloy. This is very close to the literature data (see Fig. 3). Near 200 K a weak peculiarity in the $\chi(T)$ curve is obviously observed [see the inset of Fig. 3(a)]. It is well known that the stoichiometric $Ni_2MnGa$ exhibits a martensitic transformation at $T \approx 202$ K from tetragonal to cubic phase upon warming.[40] This transformation is also accompanied by the changes in the saturation magnetization of the alloy.[41] Therefore, it may be assumed that in our case the observed peculiarity at 200 K has the same origin. However, no evidences for the phase transformation near this temperature region can be found in the $\Delta L/L$ dependence, while the magnetic transformation near $T_C$ is clearly seen [see Fig. 3(b)].

The most ordered $Ni_2MnIn$ alloy film definitely exhibits the ferromagnetic behavior with $T_C = 330$ K (see Fig. 4) and exhibits the largest (among the prepared films) effective magnetization $[4\pi M_{\text{eff}}\,(293\text{ K}) = 1790\text{ G}]$ (see Table I). Unlike the results of Xie *et al.*[42] and Dong *et al.*,[43] $T_C$ for the $L2_1$ ordered films is even slightly higher than that for the bulk alloy (see Table I). The effective magnetization of the $Ni_2MnIn$ alloy films is reduced noticeably upon $L2_1 \rightarrow B2$ structural disordering (773 and 247 G for films deposited onto substrates at 660 and 545 K, respectively) and falls down to zero for amorphous films. However, an annealing of the amorphous $Ni_2MnIn$ alloy films at 750 K for 2 h leads to their crystallization with the formation of $B2$ type of order and restores the ferromagnetic behavior with $T_C = 325$ K and $4\pi M_{\text{eff}}\,(293\text{ K}) = 743$ G (see Figs. 4 and 5). FC curves for both crystalline samples show nearly the same behavior and

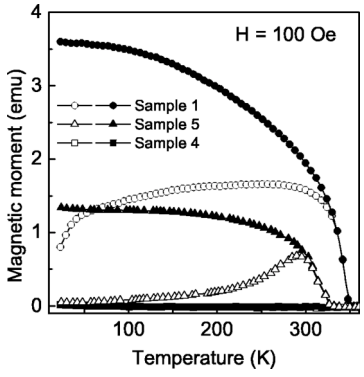


FIG. 4. Normalized with respect of film thickness ZFC (open symbols) and FC (solid symbols) in-plane magnetization curves for the $Ni_2MnIn$ alloy films.

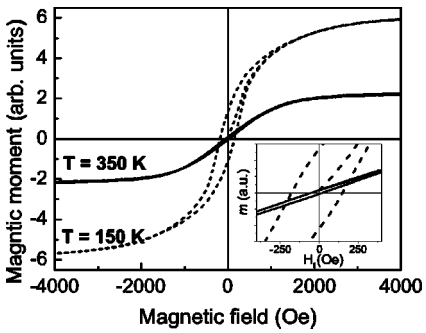


FIG. 5. In-plane magnetization hysteresis loops taken below ($T=150$ K) and above ($T=350$ K) $T_C$ for the sample 5. Inset shows the low-field part of $M(H)$ curves.

indicate larger magnetization for $L2_1$-type ordered films, while ZFC curves look noticeably different: the steeper decrease in magnetization for the sample 5 below 300 K is probably related to a less homogeneous crystalline structure of this film. It is seen that the in-plane saturation-magnetization field for the crystalline films is above 4000 Oe (see Fig. 5), while FC $M(T)$ curves were taken by SQUID only at field of 100 Oe. This might be responsible for different ratios of magnetization for the $L2_1$-and $B2$-type ordered $Ni_2MnIn$ crystalline films obtained from FMR and SQUID measurements. The amorphous films show a very small magnetization nearly independent of $T$ for both ZFC and FC measurements. Such a behavior may be attributed to Pauli paramagnetism. A similar behavior was also observed for amorphous $Ni_2MnGa$ films.[12]

The first-principles calculation of the magnetic moment for the $Ni_2MnIn$ alloy made for experimentally determined values of lattice parameters of our bulk and $L2_1$-type ordered film samples revealed 4.294 and 4.369$\mu_B$ ($\sim$3.67$\mu_B$/Mn and $\sim$0.34$\mu_B$/Ni), respectively. Since the measurement was done at RT and the applied field was not strong enough to saturate the sample, these values are significantly larger than the magnetic moment (3.57$\mu_B$) converted from $4\pi M_{eff}$ in Table I. However, these values are very close to the other experimental magnetic moment (4.34$\mu_B$) for bulk $Ni_2MnIn$ alloy with a lattice constant of 6.075 Åtaken at 4.2 K and magnetic field of 18 kOe.[44] The calculated magnetic moment in the film appeared to be larger than the moment in bulk by about 1.0%. Probably, the same (i.e., exchange splitting related) mechanism is also responsible (at least partially or indirectly) for the increase by about 3–4 % of the experimentally determined values of $T_C$ for the ordered films in comparison with that of ordered bulk sample.

### B. Optical and magneto-optical properties of alloy

The results of the optical study for bulk $Ni_2MnIn$ alloy are displayed in Fig. 6. It is seen that the measured optical properties of bulk alloy are rather sensitive to the quality of the sample surface. The OC [$\sigma(\omega)=\omega\varepsilon_2(\omega)/4\pi$, where $\varepsilon_2$ is the imaginary part of the diagonal components of DF] spectrum for the annealed bulk sample exhibits two interband-absorption peaks located at 1.7 and 3.0 eV. The 3.0 eV peak has also peculiarities (shoulders) on its high-energy slope,

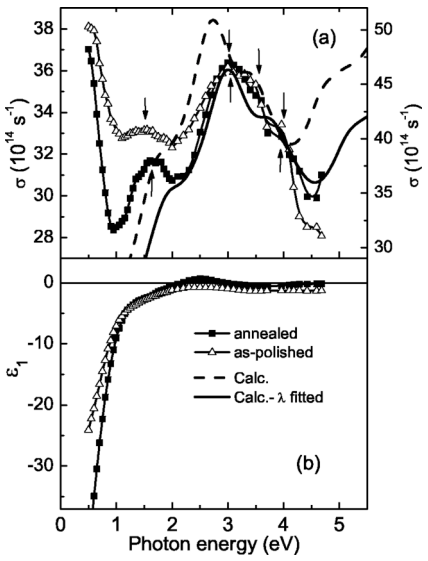


FIG. 6. (a) Experimental (left scale, triangles, and squares) and calculated (right scale, solid, and dashed curves) optical conductivity and (b) experimental $\varepsilon_1$ spectra of as-polished and annealed at 720 K for 3 h bulk $Ni_2MnIn$ alloy.

which are located at 3.5 and 4.0 eV. For $\hbar\omega<1$ eV energy range a rapid growth of $\sigma$ as well as an increase in absolute value of the real part of the diagonal components of DF, $\varepsilon_1$, (being negative) with decrease in photon energy is observed. Such a behavior is a typical manifestation of the predominance of the intraband absorption in this energy range. The OC spectrum of the as-polished bulk sample looks similar to that of the annealed one, but the interband-absorption peaks are somewhat broadened and the magnitude of the OC as a whole in the $\hbar\omega<2.5$ eV energy region is enhanced, probably owing to the enhanced scattering rate in the damaged layer of mechanically polished surface. The $\varepsilon_1$ of the as-polished sample in the near-infrared (NIR) region, still being negative, is significantly decreased in the absolute value.

The calculated OC spectra with and without the λ fitting[38] are also shown in Fig. 6. The electronic-structure calculation was done for the theoretical lattice constant, which is 6.092 Å and very close to the experimental value (about 0.26% larger than the experimental one), determined by minimizing the total energy with respect to the lattice constant. In the calculated spectra the Drude contribution was not included. The broadened spectrum has a shoulder at $\sim$1.7 eV, a peak at $\sim$2.6 eV and another shoulder at $\sim$3.5 eV. The shoulder at $\sim$1.7 eV corresponds to the peak at $\sim$1.7 eV in the experimental spectrum, the peak at $\sim$2.6 eV to the experimental 3 eV peak and the shoulder at $\sim$3.5 eV to the experimental 3.5 and 4.0 eV shoulders. Although the lowest-energy feature is well reproduced in the calculation, the calculated spectrum has the interband-absorption features at slightly lower-energy positions than the experiment. Therefore, we applied the λ fitting[38] with $\lambda=0.1$, the agreement between the experiment and calculation was much improved, especially in the high-energy region.

We further analyzed the characteristics of bands involved in each strong interband absorption. The most intense contri-

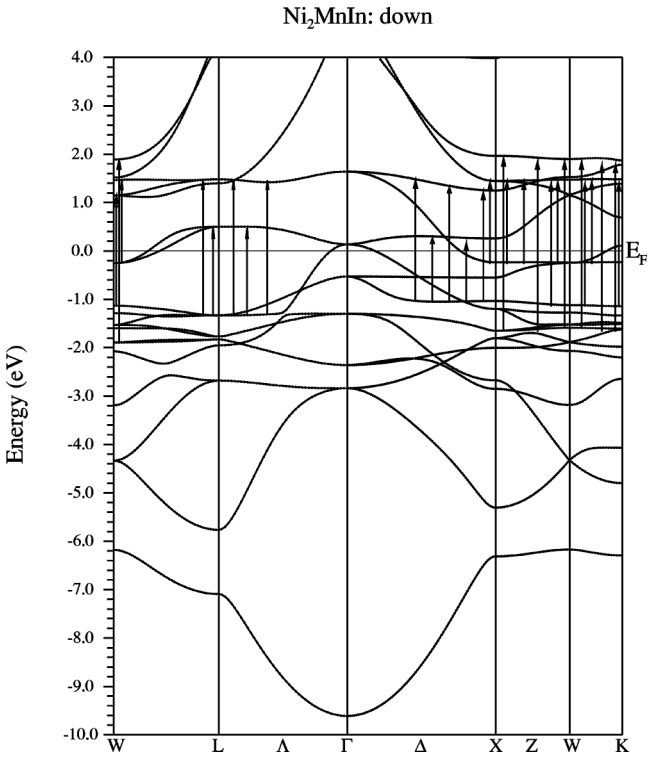


FIG. 7. Energy-band (minority) structure of the $Ni_2MnIn$ alloy along the high-symmetry lines. Intense optical transitions are indicated by arrows.

butions to the 1.7 eV shoulder are the optical transitions from the 10th minority band to the 14th minority band in the midway of the $\Gamma$-$X$ line and the 14th minority band to the 18th minority band near the $X$-$W$-$K$ plane. These optical transitions are indicated in Fig. 7 by arrows. The 10th and 14th bands have mostly the Ni $3d$ character with a small amount of $sp$ characters intermixed and the 18th band has mainly the Mn $3d$ with a considerable amount of the Ni $3d$ character. The most intense contributions to the 3.0 eV peak are the optical transitions from the 10th minority band to the 18th minority band near the $X$-$W$-$K$ plane and $L$ point. The most intense contributions to the 3.5 eV shoulder are the optical transitions from the 7th minority band to the 18th minority band near the $X$-$W$-$K$ plane. The 7th band has mostly the Ni $3d$ and Mn $3d$ characters with a small amount of $p$ characters intermixed and the 20th band has mainly the Mn $3d$ character. Since all the bands involved in the aforementioned transitions are mostly $d$ character, the dipole transitions are not so strong. However, both the initial and final bands are very flat. Therefore, we can conclude that the joint-DOS effects are responsible for these transitions. Since the majority-spin DOS is very small in the 0–4 eV range above $E_F$, the majority-spin bands contribute little to the optical transitions in the measured energy range.

Similar results of the agreement between experiments and calculations were observed for other HA. The optical properties of several true ferromagnetic HA containing Mn on $Y$ sites were theoretically examined by Kubo *et al.*[28,29] and studied experimentally by Kirillova *et al.*[31] It was shown that the OC spectra for $Cu_2MnAl$, $Pd_2MnSn$, and $Ni_2MnSn$ alloys were rather similar to each other and showed several interband-absorption peaks in the 0–7 eV energy range. The experimental OC spectrum for bulk $Ni_2MnSn$ alloy in the 0.5–4.0 eV energy range[31] is in a reasonable agreement with theory and also looks rather similar to the OC spectrum of annealed bulk $Ni_2MnIn$ sample, exhibiting two interband-absorption peaks at 1.7 and 3.3 eV.

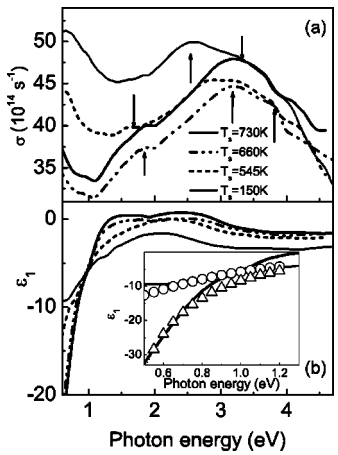


FIG. 8. Experimental (a) OC and (b) $\varepsilon_1$ spectra of the $Ni_2MnIn$ alloy films deposited at 150, 545, 660, and 730 K. Inset in panel (b) shows an extended view of the $\varepsilon_1$ spectra for the samples 1 and 4 together with fitting results.

Figure 8 shows the $\sigma(\omega)$ and $\varepsilon_1(\omega)$ spectra for the $Ni_2MnIn$ films with different degrees of structural order. It is seen that the $L2_1$-type ordered alloy film has the OC spectrum rather similar to that of annealed bulk alloy (see Figs. 6 and 8). However, the locations of both the interband-absorption peaks are blue shifted by about 0.2 eV (i.e., to 1.9 and 3.2 eV, see also Table II) and the low-energy peak is less manifested than that in the OC spectrum of annealed bulk alloy. This blue shift cannot be explained by the increase in lattice constant of the ordered film in comparison with that of bulk sample, since a lattice expansion or tetragonal distortion pushes (at least in certain directions of the reciprocal space) the energy bands above (below) $E_F$ toward the lower- (higher-) energy region.[45] As a consequence, the enlarged lattice constant should lead to the red shift, rather than blue shift, of features in the OC spectrum. Furthermore, all the investigated crystalline $Ni_2MnIn$ alloy films have practically the same lattice parameter (see Table I). Therefore, the possible reason of peak shift, which is related to the differences in lattice parameter, can safely be excluded from the consideration for the film samples.

The structural disordering (or, in other words, the decrease in the substrate temperature 730–545 K) causes a red shift of both interband-absorption peaks in the OC spectra and reduces the intensity of the low-energy one. A further increase in the structural disordering (i.e., to the amorphous sample) results in a further red shift of the high-energy peak by 0.6 eV (in comparison with the peak position in the OC spectrum of the most-ordered film sample) and disappearance of the low-energy absorption peak (see Fig. 8 and Table II). At the same time, the overall magnitude of OC in the NIR region becomes even greater than those of the ordered

TABLE II. Position of the low- (LEP) and high-energy peaks (HEP) in the OC, EKE, and $\varepsilon_2'(\hbar\omega)^2$ spectra; plasma and effective relaxation frequencies for the $Ni_2MnIn$ films deposited onto substrates at different temperatures.

| | OC | | EKE | | $\varepsilon_2'(\hbar\omega)^2$ | | | |
|---|---|---|---|---|---|---|---|---|
| $T_s$ (K) | LEP (eV) | HEP (eV) | LEP (eV) | HEP (eV) | LEP (eV) | HEP (eV) | $\Omega_P^2$ ($10^{32}$ $s^{-2}$) | $\gamma$ ($10^{14}$ $s^{-1}$) |
| 150 | | 2.60 | | | | | 0.23 | 10.6 |
| 545 | 1.60 | 2.80 | | | | | | |
| 660 | 1.86 | 3.18 | 1.63 | 2.92 | 1.47 | 2.79 | | |
| 730 | 1.90 | 3.20 | 1.63 | 2.98 | 1.48 | 2.76 | 0.22 | 2.2 |
| Bulk | 1.62 | 3.02 | 1.58 | 2.83 | 1.42 | 2.56 | | |

states probably because of the enhanced scattering rate of charge carriers. It is clear that the observed HEP shift is not related with the changes in lattice constants.

It is well known that the main source of the magnetic moment in the ordered ferromagnetic Mn-containing HA is from the Mn atoms, and that the contribution from *X*-transition metal is relatively small. Our calculated magnetic moments are $3.67\mu_B$/Mn and $0.34\mu_B$/Fe. Negligibly small amounts of magnetization were found in the interstitial region and Ga atom. The lack of ferromagnetic order in the amorphous state of $Ni_2MnIn$ alloy indicates the lack of exchange interaction among the Mn atoms and hence a redistribution in the DOS of the Mn atoms, in comparison with that of the ferromagnetic state, has taken place.[12] In Fig. 7, the Mn $3d$ minority bands located at $\sim$1.4 eV above $E_F$ are the final states for the low-energy and high-energy interband-absorption peaks. Thus, from this point of view, a noticeable change in both peaks due to structural disordering (or more definitely due to lack of exchange splitting) might also be expected. Furthermore, it is clear that $E_F$ will also be somehow shifted in order to maintain the electron concentration invariant. The initial states for the low-energy peak are located at either $\sim$0.2 eV (near the *X*-*W*-*K* plane) or $\sim$1.2 eV (near the *L* point) below $E_F$. Thus, the experimentally observed weakening of the low-energy peak and the red shift of the high-energy peak in the OC spectrum of the disordered (nonmagnetic) $Ni_2MnIn$ alloy can be explained by emptying the Ni $3d$ minority bands near the *X*-*W*-*K* plane and by changes in Mn $3d$ minority bands, which are located at $\sim$1.4 eV above $E_F$ for the ordered case.

It is seen that below 1 eV the $\varepsilon_1(\omega)$ and $\sigma(\omega)$ spectra for all the investigated samples look Drude-like. Frequency dependence of $\varepsilon_1$ in the region of intraband absorption may be expressed as

$$\varepsilon_1 = 1 - \frac{\Omega_P^2}{(\omega^2+\gamma^2)},$$

where $\Omega_P$ and $\gamma$ are plasma and effective relaxation frequencies of free charge carriers. After a simple transformation this dependence might be presented as

$$\frac{1}{(1-\varepsilon_1)} = \frac{\gamma^2}{\Omega_P^2} + \frac{1}{\Omega_P^2}\times\omega^2.$$

The linear part of the experimental $1/(1-\varepsilon_1)$ vs $\omega^2$ plots is interpreted as the region of free-electron absorption. The $\Omega_P$ and $\gamma$ were determined for the most ordered and disordered states by least-square fitting of the $1/(1-\varepsilon_1)$ vs $\omega^2$ plots. It was found that $\Omega_P^2$ ($\Omega_P^2 = 4\pi Ne^2/m^*$, where $N$ and $m^*$ are the charge-carrier concentration and the effective mass, respectively) is practically unchanged upon the structural disordering, while $\gamma$ increases nearly five times (see Table II). This means that the DOS at $E_F$ and $m^*$ are insensitive to the structural disordering, but the scattering processes are enhanced. The validity of obtained results was proven by the simulation of the $\varepsilon_1(\omega)$ spectra with the determined $\Omega_P$ and $\gamma$ as input parameters (see inset in Fig. 8).

Comparing the OC spectra of the as-polished and annealed bulk samples as well as the disordered and ordered film samples, a question may occur: *Why the OC as a whole in the NIR region for as-polished bulk or amorphous film is larger than those for annealed bulk and crystalline film samples?* Two factors may be responsible for the OC spectra enhancement in the NIR region. First, the broadening of interband-absorption peaks for the as-polished or amorphous phases is responsible for the weakened peaks and enhanced background or plateau for the rest part of the spectrum. Second, the increase in scattering processes on the defects of the surface layers leads to the enhanced OC in the NIR region. This process finds its manifestation in an increase of the effective relaxation frequency $\gamma$ and, hence, in a larger contribution to the resultant OC in the visible region from the tail of the Drude term.

The EKE spectra for the most ordered $Ni_2MnIn$ alloy film ($T_s = 730$ K) and the bulk sample manifest two negative peaks and a narrow intense positive peak in the NIR region (see Fig. 9). These peaks in the EKE spectra are located at somewhat smaller energies than interband-absorption peaks in the corresponding OC spectra (see Table II). A similar regularity in the OC spectra is also observed in the relative positions of peaks in the EKE spectra for the bulk sample and the most ordered film. The origin of this shift is probably the same as the shift in the OC spectra, and relevant to the deviation from stoichiometry in the film samples. The structural disordering to the $B2$ type leads to a very rapid decrease in the magnitude of the MO effect, and the EKE for amorphous $Ni_2MnIn$ alloy films was not detected at all. The EKE spectrum of the crystalline $Ni_2MnIn$ alloy films with

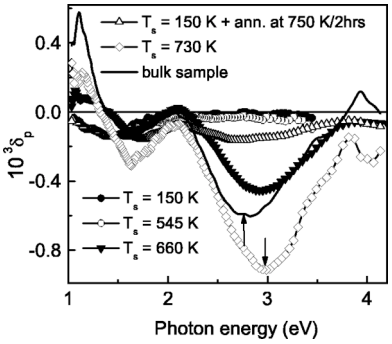


FIG. 9. Experimental EKE spectra for the $Ni_2MnIn$ alloy bulk and film samples deposited at 150, 545, 660, and 730 K taken at $\varphi = 75°$ and $T = 293$ K.

$B2$-type order (which were formed by an annealing of the amorphous films) also exhibits a negative double-peak structure, although its intensity is rather small. Figure 10 shows the substrate-temperature dependence of the $4\pi M_{\text{eff}}$, $-\delta_{\text{p}}$, and $\sigma$ for $Ni_2MnIn$ alloy films. $-\delta_{\text{p}}$ and $\sigma$ are the values at the energies corresponding to the high-energy maximum in EKE spectra. It can be concluded that the magnitude of MO response of the films is determined mainly by their magnetization, and for the determination of the EKE value the optical constants may play some role, but not significant. These arguments are based on the fact that the optical constants are rather insensitive to the substrate temperature and the substrate-temperature dependence of the EKE value at the high-energy maximum exactly follows the corresponding dependence of the effective magnetization (see Fig. 10).

The off-diagonal components of DF for the bulk and the most crystalline film were calculated by using the results of EKE measurements at two angles of incidence and experimentally determined optical constants of the corresponding bulk and film samples. The spectra of absorptive part of the off-diagonal components also show a negative double-peak structure (see Fig. 11). The locations of these peaks are red shifted by about 0.4 eV in comparison with those in the OC spectra of the corresponding crystalline samples. The calculated spectrum after broadening and λ fitting with $\lambda = 0.10$ is also included in Fig. 11. As can be seen in Fig. 11, the calculated spectrum could excellently reproduce the experimental spectrum, except for the magnitude. Similar arguments given in the discussion of the calculated OC spectrum can be applied to the case of the calculated off-diagonal component of OC tensor.

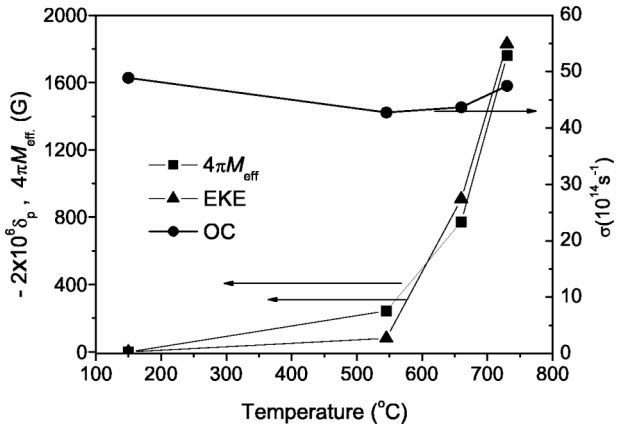


FIG. 10. The substrate-temperature dependence of the effective magnetization, the EKE and OC values at the energies corresponding to the high-energy maximum in EKE spectra.

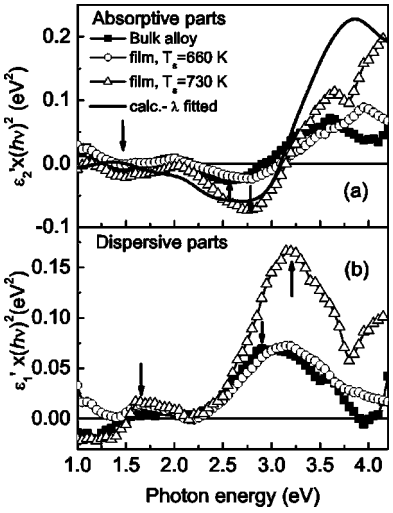


FIG. 11. (a) Absorptive $[\varepsilon_2' \times (\hbar\omega)^2]$ and (b) dispersive $[\varepsilon_1' \times (\hbar\omega)^2]$ parts of the off-diagonal components of the DF for bulk and $L2_1$- and $B2$-type ordered films of $Ni_2MnIn$ alloy. Broadened and λ-fitted spectrum (calculated) is also shown (scaling factor $= 1/20$).

## V. SUMMARY

The ordered $Ni_2MnIn$ films with a $T_C$ close to the literature data for the ordered stoichiometric bulk alloy were fabricated. The diagonal and off-diagonal components of DF for the crystalline $Ni_2MnIn$ alloy were experimentally determined. Both diagonal and off-diagonal spectra of the optical-conductivity tensor were also calculated by using WIEN2K code and the agreement between experiments and calculations was reasonable after the so-called λ fitting. The most intense optical transitions occur between the minority-spin bands with mostly Ni and/or Mn $3d$ characters and the joint-density-of-states effects are responsible for these transitions. The changes in the electronic structure in $Ni_2MnIn$ alloy caused by the structural disordering were elucidated on the basis of the results of the experimental and theoretical optical and MO studies. It was shown that the structural transformations, $L2_1 \rightarrow B2$ and then $B2 \rightarrow$ amorphous state, lead, at first, to a decrease and then to disappearance of the ferromagnetic order. The changes in the electron-energy structure of alloy near the Fermi level caused by atomic disordering also destroy (or make worse) the band matching of the $Ni_2MnIn$ alloy to, for example, InAs layer. Both these factors make worse the figure of merit of $Ni_2MnIn$ alloy layers as spin injector. An annealing at 750 K for 2 h of the amorphous films restores the $B2$-type crystalline structure and recovers the ferromagnetic order.

**ACKNOWLEDGMENTS**

This work was supported by the KOSEF through Quantum Photonic Science Research Center, by a Korea Research Foundation Grant (Grant No. KRF-99-D00048), and by MOST, Korea. We are also grateful to J. Dubowik for his help with the magnetic measurements and to Y. N. Petrov for the TEM study of the film samples.

*Electronic address: yplee@hanyang.ac.kr

[1] I. Galanakis, Scientific Highlight of the Month, $\Psi_k$ Newsletter **51**, 105 (2002).
[2] P.R. Hammar, B.R. Bennett, M.J. Yang, and M. Johnson, Phys. Rev. Lett. **83**, 203 (1999).
[3] D. Orgassa, H. Fujiwara, T.C. Schulthess, and W.H. Butler, Phys. Rev. B **60**, 13237 (1999).
[4] M. Pugacheva and A. Jezierski, J. Magn. Magn. Mater. **151**, 202 (1995).
[5] J. Kudrnovský, S.K. Bose, and O. Jepsen, Phys. Rev. B **43**, 14 409 (1991).
[6] U. Geiersbach, A. Bergmann, and K. Westerholt, J. Magn. Magn. Mater. **240**, 546 (2002).
[7] U. Geiersbach, A. Bergmann, and K. Westerholt, Thin Solid Films **425**, 225 (2003).
[8] K. Ikeda and S. Takahashi, Phys. Rev. B **30**, 3808 (1984).
[9] J. Schaf, K. Le Dang, P. Veillet, and I.A. Campbell, J. Phys. F: Met. Phys. **13**, 1311 (1983).
[10] R.C. Taylor and C.C. Tsuei, Solid State Commun. **41**, 503 (1982).
[11] L. Krusin-Elbaum, A.P. Malozemoff, and R.C. Taylor, Phys. Rev. B **27**, 562 (1983).
[12] J.Y. Rhee, Y.V. Kudryavtsev, J. Dubowik, and Y.P. Lee, J. Appl. Phys. **93**, 5527 (2003).
[13] A. Ślebarski, M.B. Maple, E.J. Freeman, C. Sirvent, D. Tworuszka, M. Orzechowska, A. Wrona, A. Jezierski, S. Chiuzbaian, and M. Neumann, Phys. Rev. B **62**, 3296 (2000).
[14] G.L.F. Fraga, J.V. Kunzler, F. Ogiba, and D.E. Brandão, Phys. Status Solidi A **83**, K188 (1984).
[15] P.J. Webster, K.R.A. Ziebeck, S.L. Town, and M.S. Peak, Philos. Mag. B **49**, 295 (1984).
[16] C.M. Hurd and S.P. McAlister, J. Magn. Magn. Mater. **61**, 114 (1986).
[17] K.A. Kilian and R.H. Victora, J. Appl. Phys. **87**, 7064 (2000).
[18] P.A.M. van der Heide, W. Baelde, R.A. de Groot, A.R. de Vroomen, P.G. van Engen, and K.H.J. Buschow, J. Phys. F: Met. Phys. **15**, L75 (1985).
[19] R. Ohyama, T. Koyanagi, and K. Matsubara, J. Appl. Phys. **61**, 2347 (1987).
[20] M. Naoe, N. Kitamura, M. Shoji, and A. Nagai, J. Appl. Phys. **63**, 3636 (1998).
[21] H. Fu, Z. Yan, S.K. Lee, and M. Mansuripur, J. Appl. Phys. **78**, 4076 (1995).
[22] E. Kulatov, Yu. Uspenskii, and S. Halilov, J. Magn. Magn. Mater. **145**, 395 (1995).
[23] J.F. Bobo, P.R. Johnson, M. Kautzky, F.B. Mancoff, E. Tuncel, R.L. White, and B.M. Clemens, J. Appl. Phys. **81**, 4164 (1997).
[24] V.N. Antonov, P.M. Oppeneer, A.N. Yaresko, A.Ya. Perlov, and T. Kraft, Phys. Rev. B **56**, 13 012 (1997).
[25] J.A. Caballero, W.J. Geerts, F. Petroff, J.-U. Thiele, D. Weller, and J.R. Childress, J. Magn. Magn. Mater. **177–181**, 1229 (1998).
[26] X. Gao, J.A. Woollam, R.D. Kirby, D.J. Sellmyer, C.T. Tanaka, J. Nowak, and J.S. Moodera, Phys. Rev. B **59**, 9965 (1999).
[27] V.N. Antonov, A.N. Yaresko, A.Ya. Perlov, V.V. Nemoshkalenko, P.M. Oppeneer, and H. Eschrig, Low Temp. Phys. **25**, 387 (1999).
[28] Y. Kubo, S. Ishida, and J. Ishida, J. Phys. F: Met. Phys. **11**, 2443 (1981).
[29] Y. Kubo, N. Takakure, and S. Ishida, J. Phys. F: Met. Phys. **13**, 161 (1983).
[30] E.I. Shreder, M.M. Kirillova, and V.P. Dyakina, Fiz. Met. Metalloved. **81**, 82 (1996) (in Russian).
[31] M.M. Kirillova, Yu.I. Kuz'min, Yu.V. Knyazev, and E.I. Shreder, Phys. Met. Metallogr. **83**, 590 (1997).
[32] J. van Ek, W. Huang, and J.M. MacLaren, J. Appl. Phys. **81**, 5429 (1997).
[33] E.I. Shreder, M.M. Kirillova, and V.P. Dyakina, Fiz. Met. Metalloved. **90**, 48 (2000) (in Russian).
[34] P. Blaha, K. Schwarz, G.K.H. Madsen, D. Kvasnicka, and J. Luitz, *WIEN2k, An Augmented Plane Wave + Local Orbitals Program for Calculating Crystal Properties* (Karlheinz Schwarz, Techn. Universität Wien, Wien, 2001).
[35] E. Wimmer, H. Krakauer, M. Weinert, and A.J. Freeman, Phys. Rev. B **24**, 864 (1981).
[36] J.P. Perdew, K. Burke, and M. Ernzerhof, Phys. Rev. Lett. **77**, 3865 (1996).
[37] J.Y. Rhee, J. Korean Phys. Soc. **43**, 792 (2003).
[38] J.Y. Rhee, B.N. Harmon, and D.W. Lynch, Phys. Rev. B **55**, 4124 (1997).
[39] J.Y. Rhee, B.N. Harmon, and D.W. Lynch, Phys. Rev. B **54**, 17 385 (1996).
[40] A.N. Vasil'ev, A.D. Bozhko, V.V. Khovailo, I.E. Dikshtein, V.G. Shavrov, V.D. Buchelnikov, M. Matsumoto, S. Suzuki, T. Takagi, and J. Tani, Phys. Rev. B **59**, 1113 (1999).
[41] F. Zuo, X. Su, and K.H. Wu, Phys. Rev. B **58**, 11 127 (1998).
[42] J.Q. Xie, J.W. Dong, J. Lu, C.J. Palmstrøm, and S. McKernan, Appl. Phys. Lett. **79**, 1003 (2001).
[43] J.W. Dong, J. Lu, J.Q. Xie, L.C. Chen, R.D. James, S. McKernanm, and C.J. Palmstrøm, Physica E (Amsterdam) **10**, 428 (2001).
[44] K.H.J. Buschow, P.G. van Engen, and R. Jongebreur, J. Magn. Magn. Mater. **38**, 1 (1983).
[45] J.Y. Rhee, Y.V. Kudryavtsev, Y.P. Lee, and K.W. Kim, J. Korean Phys. Soc. **36**, 404 (2000).